Article

Perforated Layer Structures in Liquid Crystalline Rod–Coil Block Copolymers

Kishore K. Tenneti, Xiaofang Chen, Christopher Y. Li, Yingfeng Tu, Xinhua Wan, Qi-Feng Zhou, Igors Sics, and Benjamin S. Hsiao

J. Am. Chem. Soc., **2005**, 127 (44), 15481-15490• DOI: 10.1021/ja053548k • Publication Date (Web): 13 October 2005

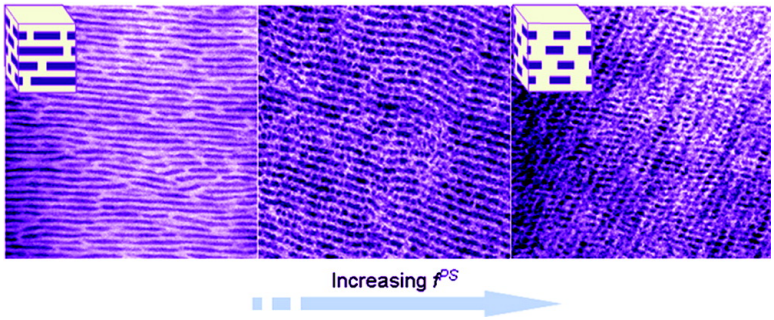

J|A|C|S
ARTICLES
Published on Web 10/13/2005

Perforated Layer Structures in Liquid Crystalline Rod−Coil Block Copolymers

Kishore K. Tenneti,[†] Xiaofang Chen,[†,‡] Christopher Y. Li,*[,†] Yingfeng Tu,[‡] Xinhua Wan,*[,‡] Qi-Feng Zhou,*[,‡] Igors Sics,[§] and Benjamin S. Hsiao[§]

Contribution from the A. J. Drexel Nanotechnology Institute and Department of Materials Science and Engineering, Drexel University, Philadelphia, Pennsylvania 19104, Department of Polymer Science and Engineering, College of Chemistry, Peking University, Beijing, P. R. China, 100871, and Department of Chemistry, State University of New York at Stony Brook, Stony Brook, New York 11794

Received May 31, 2005; E-mail: chrisli@drexel.edu; xhwan@pku.edu.cn; qfzhou@pku.edu.cn

Abstract: We report a novel observation of the tetragonal perforated layer structures in a series of rod−coil liquid crystalline block copolymers (BCPs), poly(styrene-*block*-(2,5-bis[4-methoxyphenyl]oxycarbonyl)-styrene) (PS-*b*-PMPCS). PMPCS forms rigid rods while PS forms the coil block. Differential scanning calorimetry (DSC), polarized light microscopy (PLM), small-angle X-ray scattering (SAXS), wide-angle X-ray diffraction (WAXD), and transmission electron microscopy (TEM) techniques were used to investigate these rod−coil molecules, and a perforated layer structure was observed at $f^{PMPCS} \approx 0.37$ in relatively low molecular weight (M_w) samples and ~0.5 in high M_w PS-*b*-PMPCS. This substantial phase boundary shift was attributed to the rod−coil nature of the BCP. The perforation obeys a tetragonal instead of hexagonal symmetry. The "onset" of perforation was also observed in real space in sample PS_{272}-*b*-$PMPCS_{93}$ ($f^{PMPCS} \approx 0.52$), in which few PS chains punctuate PMPCS layers. A slight increase in f^{PS}, by blending with PS homopolymer, led to a dramatic change in the BCP morphology, and uniform tetragonal perforations were observed at $f^{PMPCS} \approx 0.48$.

Introduction

Block copolymer (BCP) self-assembly is an essential part of nanotechnology, and it offers one of the few practical strategies for making ensembles of nanostructures.[1,2] Self-assembled BCPs have found applications in a number of fields of nanotechnology such as photonic band gap materials, nanostructured networks, nanolithographic templates, etc.[3−5] Most of the research in this field has been focused on coil−coil BCPs with flexible polymer chains.[6−8] During the past two decades, rod−coil BCPs, where one of the combining blocks has a rigid conformation and the other is flexible, have attracted great attention.[2,9−13] Due to the combination of two extreme polymer chain conformations (rigid and flexible), complex phase structures and morphologies have been observed.[11] For instance, relatively symmetric BCPs lead to the simplest lamellar morphology, while, in the case of rod−coil BCPs, seven different lamellar phases [monolayer smectic A (Sm_A), bilayer Sm_A, bilayer smectic C (Sm_C), smectic B, smectic E, smectic F, and smectic O (Sm_O)] have been reported, depending on different packing schemes of the rods.[9,14] Phase structures of coil−coil BCPs are dictated by the Flory−Huggins parameter χ and the volume fraction of one block (f). In rod−coil BCPs, in addition to these two parameters, the properties of rod blocks are also critical to the final phase formation. Packing of the rod and coil blocks at the interface is generally controlled by the volume fraction of the coil (f^{coil}) as well as the *area per junction* of the coil (A^{coil}) and the rod (A^{rod}). Complex phases, such as sphere and double gyroid phases, have been observed only in the low molecular weight (M_w) oligomer systems.[10] As the M_w of the rod segment increases, the length of the rods increases. These longer rods prefer flat intermaterial dividing surface (IMDS), and packing such rods within highly curved IMDS in sphere or double gyroid phases could generate packing defects and increase the packing energy. Consequently, some highly asymmetric rod−coil BCPs also show smectic phases.[11] If A^{coil} is larger than A^{rod}, the coils are densely packed at the interface, which in turn results in the stretching of the

[†] Drexel University.
[‡] Peking University.
[§] State University of New York at Stony Brook.

(1) Ikkala, O.; Brinke, G. T. *Science* **2002**, *295*, 2407−2409.
(2) Muthukumar, M.; Ober, C. K.; Thomas, E. L. *Science* **1997**, *277*, 1225−1232.
(3) Forster, S.; Plantenberg, T. *Angew. Chem., Int. Ed.* **2002**, *41*, 688−714.
(4) Liu, T.; Burger, C.; Chu, B. *Prog. Polym. Sci.* **2003**, *28*, 5−26.
(5) Park, C.; Yoon, J.; Thomas, E. L. *Polymer* **2003**, *44*, 6725−6760.
(6) Hamley, I. W. *The Physics of Block Copolymers*; Oxford University Press: Oxford, 1998.
(7) Bates, F. S. *Science* **1991**, *251*, 898−905.
(8) Bates, F. S.; Fredrickson, G. H. *Annu. Rev. Phys. Chem.* **1990**, *41*, 525−557.
(9) Gallot, B. *Prog. Polym. Sci.* **1996**, *21*, 1035−1088.
(10) Lee, M.; Cho, B. K.; Zin, W. C. *Chem. Rev.* **2001**, *101*, 3869−3892.
(11) Chen, J. T.; Thomas, E. L.; Ober, C. K.; Mao, G. P. *Science* **1996**, *273*, 343−346.
(12) Mao, G. P.; Ober, C. K. Block copolymers containing liquid crystalline segments. In *Handbook of Liquid Crystals*; Demus, D., Goodby, J., Gray, G. W., Spiess, H. W., Eds.; Wiley-VCH: 1998; Vol. 3.
(13) Deming, T. J. *Adv. Mater.* **1997**, *9*, 299−311.

(14) Note that, according to the LC nomenclature, the lamellar phase of rod-coils BCPs is considered as a smectic phase.

coils along the IMDS normal. Interdigitation and tilting of the rods could occur.[11] In addition, the rod length/diameter ratio also plays an important role in the rod−coil BCP phase formation.

A number of theoretical results on possible phase structures have also been reported. Nematic, monolayer Sm_A, bilayer Sm_A, and Sm_C have been investigated.[15] An interesting hockey puck structure was proposed by Williams et al. for the rod−coil BCPs with high f^{coil}.[16] Müller et al. showed that the stable morphologies of rod−coil BCPs should have the coils on the convex side of the rod−coil interface.[17] Recently, lamellar, zigzag lamellar, elliptical cross-sectional cylinders, hexagonally packed cylinders have also been investigated.[18−22]

At least three different types of rod structures have been used to construct the rigid block for rod−coil BCPs. These include polypeptides,[9,23−27] liquid crystal (LC)/conjugated oligomers,[10,24,28,29] and poly(hexyl isocyanate) (PHIC) and it derivatives.[11,30,31] Polypeptides [such as poly (γ-benzyl-L-glutamate (PBLG), poly(z-L-Lysine), poly(L-valine), poly(L-leucine), etc.][9,23,25−27,32,33] form an α-helix conformation with a relatively long persistent length (rigid rod) and were first used as the rod block in rod−coil BCPs. The phases that were observed in these rods are nematic, columnar, cubic, and lamellar. The coil blocks that have been employed include polystyrene, poly(isoprene), poly(butadiene), poly(dimethylsiloxane), poly(ethylene oxide), and poly(propylene oxide).[9,23,25−27,32] Rod−coil BCPs containing polypeptide oligomers (degree of polymerization ∼10−80) were also studied by FTIR and small-angle X-ray scattering (SAXS).[23] In addition to the lamellar phase, columnar hexagonal and double hexagonal structures have also been observed.[24] The second type of rod structures that have been employed consists of LC and conjugated oligomers. A number of research groups have investigated several elegant systems with well-designed rod−coil oligomers leading to interesting structures such as striped, hexagonal superlattice, "mushroom", Sm_A, bicontinuous cubic, hexagonal columnar, body-centered cubic structures, etc.[10,24,34,35] Recently, using PHIC as the rod block, Thomas et al. studied the structure and phase behavior of PS-*b*-PHIC.[11] PHIC forms only an α-helical conformation, and the persistent chain length is ∼50−60 nm, which can be used as the rod block. Compared to the polypeptide chains, using PHIC as the rod block is advantageous since, in the case of polypeptides, both α-helix and β-sheet conformations are possible and the latter destroys the rod conformation and leads to possible confusion in structure interpretation. A series of PS-*b*-PHIC with f^{PS} ranging from 0.02 to 0.58 have been investigated. Novel microdomain structures such as lenticular aggregates[36] (also known as wavy lamellae),[11] zigzag lamellar[37] (resembling LC Sm_C phase), and arrowhead (resembling LC Sm_O) have been observed. Formation of these complex phase structures is believed to be a result of the interplay between microphase separation of the blocks and LC transitions. Recently, both unique polymer brushes and hierarchical ordering spanning three orders of size scales [crystals of the rod block (1 nm), BCP microdomains (∼50 nm) and Nèel domain wall (∼1000 nm)] have been reported for a rod−coil poly[styrene-*block*-(triethoxysilyl)propylisocyanate].[30,31]

By laterally linking the "waist" of LC mesogens *directly* to polymer backbones (without spacers), mesogen jacketed liquid crystalline polymers (MJLCPs) can be achieved.[38−42] In most of the MJLCP systems, rigid columns of the mesogens are formed due to the strong interaction between the side chain mesogens and the polymer backbone. The mesogens are tilted with respect to the columnar axes. These rigid columns pack together forming a columnar nematic (Φ_N)/hexagonal (Φ_H) phase, and it is these supramolecular columns, rather than the individual mesogens, that possess the orientational order.[43−46] The rigid nature enables the MJLCPs to serve as rods and form a new type of *rod−coil* block copolymers. Morphology and rheological behavior of rod−coil poly(styrene)-*block*-poly(2,5-bis-(4-butyl-benzoyl)oxystyrene) (PS-*b*-PBBOS) have been reported by Ober et al.[47,48] Recently, a series of MJLCP based rod−coil block copolymers, poly(styrene-*block*-(2,5-bis[4-methoxyphenyl]oxycarbonyl)styrene) (PS-*b*-PMPCS), have been synthesized, and their solution self-assembly behavior has been investigated.[49] PMPCS based triblock and star block copolymers have also been synthesized.[50,51] In the dilute PS-*b*-PMPCS solution using xylene or cholorobenzene as solvent, PS-*b*-PMPCS forms micelles having a 20−40 nm diameter with a PMPCS core surrounded by the PS corolla. The size of the

(15) Semenov, A. N. *Mol. Cryst. Liq. Cryst.* **1991**, *209*, 191−199.
(16) Willams, D. R. M.; Fredrickson, G. H. *Macromolecules* **1992**, *25*, 3561−3568.
(17) Muller, M.; Schick, M. *Macromolecules* **1996**, *29*, 8900−8903.
(18) Li, W.; Gersappe, D. *Macromolecules* **2001**, *34*, 6783−6789.
(19) Matsen, M. W.; Barrett, C. *J. Chem. Phys.* **1998**, *109*, 4108−4118.
(20) Halperin, A. *Macromolecules* **1990**, *23*, 2724−2731.
(21) Pryamitsyn, V.; Ganesan, V. *J. Chem. Phys.* **2004**, *120*, 5824−5838.
(22) Buhot, A.; Halperin, A. *Phys. Rev. Lett.* **2000**, *84*, 2160−2163.
(23) Klok, H. A.; Langenwalter, J. F.; Lecommandoux, S. *Macromolecules* **2000**, *33*, 7819−7826.
(24) Klok, H. A.; Lecommandoux, S. *Adv. Mater.* **2001**, *13*, 1217−1229.
(25) Lecommandoux, S.; Achard, M. F.; Langenwalter, J. F.; Klok, H. A. *Macromolecules* **2001**, *34*, 9100−9111.
(26) Minich, E. A.; Nowak, A. P.; Deming, T. J.; Pochan, D. J. *Polymer* **2004**, *45*, 1951−1957.
(27) Nowak, A. P.; Breedveld, V.; Pakstis, L.; Ozbas, B.; Pine, D. J.; Pochan, D. J.; Deming, T. J. *Nature* **2002**, *417*, 424−428.
(28) Jenekhe, S. A.; Chen, X. L. *Science* **1998**, *279*, 1903−1907.
(29) Stupp, S. I. *Curr. Opin. Colloid Interface Sci.* **1998**, *3*, 20−26.
(30) Park, J. W.; Thomas, E. L. *Adv. Mater.* **2003**, *15*, 585−588.
(31) Park, J. W.; Thomas, E. L. *J. Am. Chem. Soc.* **2002**, *124*, 514−515.
(32) Schlaad, H.; Smarsly, B.; Losik, M. *Macromolecules* **2004**, *37*, 2210−2214.
(33) Babin, J.; Rodriguez-Hernandez, J.; Lecommandoux, S.; Klok, H.-A.; Achard, M.-F. *Faraday Discuss.* **2004**, *2005*, 179−192.
(34) Jenekhe, S. A.; Chen, X. L. *Science* **1999**, *283*, 372−375.
(35) Lee, M.; Cho, B. K.; Ihn, K. J.; Lee, W. K.; Oh, N. K.; Zin, W. C. *J. Am. Chem. Soc.* **2001**, *123*, 4647−4648.
(36) Chen, J. T. PhD Thesis. PhD, MIT, 1997.
(37) Chen, J. T.; Thomas, E. L.; Ober, C. K.; Hwang, S. S. *Macromolecules* **1995**, *28*, 1688−1697.
(38) Zhou, Q. F.; Zhu, X. L.; Wen, Z. Q. *Macromolecules* **1989**, *22*, 491−493.
(39) Zhang, D.; Liu, Y. X.; Wan, X. H.; Zhou, Q. F. *Macromolecules* **1999**, *32*, 5183−5185.
(40) Wan, X.; Tu, Y. F.; Zhang, D.; Zhou, Q. F. *Chin. J. Polym. Sci.* **1998**, *16*, 377−380.
(41) Pragliola, S.; Ober, C. K.; Mather, P. T.; Jeon, H. G. *Macromol. Chem. Phys.* **1999**, *200*, 2338−2344.
(42) Gopalan, P.; Ober, C. K. *Macromolecules* **2001**, *34*, 5120−5124.
(43) Tu, H.; Wan, X.; Liu, Y.; Chen, X.; Zhang, D.; Zhou, Q.-F.; Shen, Z.; Ge, J. J.; Jin, S.; Cheng, S. Z. D. *Macromolecules* **2000**, *33*, 6315−6320.
(44) Yin, X.-Y.; Ye, C.; Ma, X.; Chen, E.-Q.; Qi, X.-Y.; Duan, X.-F.; Wan, X.-H.; Cheng, S. Z. D.; Zhou, Q.-F. *J. Am. Chem. Soc.* **2003**, *125*, 6854−6855.
(45) Ye, C.; Zhang, H. L.; Huang, Y.; Chen, E. Q.; Lu, Y. L.; Shen, D. Y.; Wan, X. H.; Shen, Z. H.; Cheng, S. Z. D.; Zhou, Q. F. *Macromolecules* **2004**, *37*, 7188−7196.
(46) Shen, Y.; Chen, E. Q.; Ye, C.; Zhang, H. L.; Wu, P. Y.; Noda, I.; Zhou, Q. F. *J. Phys. Chem. B* **2005**, *109*, 6089−6095.
(47) Gopalan, P.; Li, X. F.; Li, M. Q.; Ober, C. K.; Gonzales, C. P.; Hawker, C. J. *J. Polym. Sci., Part A: Polym. Chem.* **2003**, *41*, 3640−3656.
(48) Gopalan, P.; Zhang, Y. M.; Li, X. F.; Wiesner, U.; Ober, C. K. *Macromolecules* **2003**, *36*, 3357−3364.
(49) Tu, Y. F.; Wan, X. H.; Zhang, D.; Zhou, Q. F.; Wu, C. *J. Am. Chem. Soc.* **2000**, *122*, 10201−10205.
(50) Wang, X. Z.; Zhang, H. L.; Mao, S.; Wang, X. Y.; Zhou, Q. F. *J. Polym. Sci., Part A: Polym. Chem.* **2005**, *43*, 733−741.
(51) Yi, Y.; Fan, X. H.; Wan, X. H.; Li, L.; Zhao, N.; Chen, X. F.; Xu, J.; Zhou, Q. F. *Macromolecules* **2004**, *37*, 7610−7618.

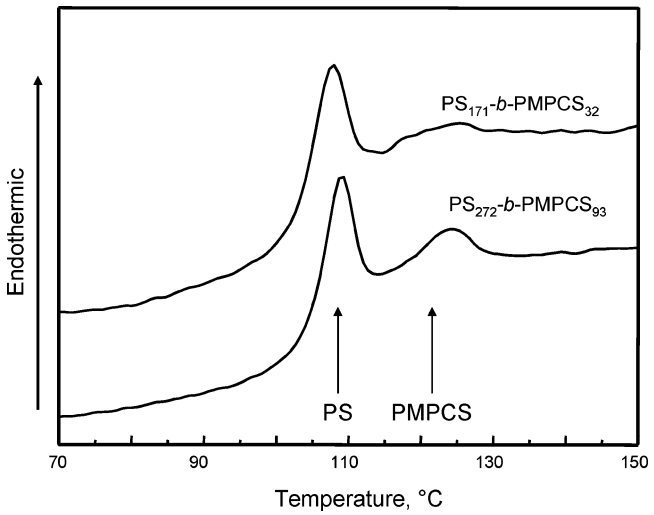

Figure 1. DSC thermograms of PS_{171}-*b*-$PMPCS_{32}$ and PS_{272}-*b*-$PMPCS_{93}$ with a heating rate of 40 °C/min (samples were cooled at 2 °C/min from 220 °C). Two hysteresis peaks of PS and PMPCS blocks can be clearly observed in both the block copolymers, indicating two glass transitions of phase separated PS and PMPCS blocks.

micelles can be controlled by the PS-*b*-PMPCS M_w. The bulk behavior of this unique rod−coil system is also intriguing. For a series of symmetric PS-*b*-PMPCS with relatively low M_w, the lamellar phase has been observed with the supramolecular PMPCS rods aligning parallel to the lamellar normal. Each LC layer consists of approximately two layers of PMPCS, and a bilayer Sm_A phase was thus proposed.[52]

In this paper, we report our observation of a perforated layer (PL) structure in both low M_w asymmetric and high M_w symmetric PS-*b*-PMPCS BCPs where the PS chains perforate the PMPCS layers. In these PL forming systems, PS is the major component (with $f^{PS} \approx 0.63$) in the low M_w BCPs while f^{PS} is ~0.5 in high M_w BCPs. More interestingly, SAXS experiments show the perforation of the PS into PMPCS layers obeys a tetragonal, instead of the conventional hexagonal, symmetry. f^{PS} was fine-tuned by blending PS-*b*-PMPCS with a lower M_w PS homopolymer, and it was found that the "degree" of perforation increased with increasing f^{PS}.

Results and Discussion

Perforated Layer Structure of PS-*b*-PMPCS. The first PS-*b*-PMPCS BCP that was investigated in this study is PS_{171}-*b*-$PMPCS_{32}$, with $f^{PMPCS} \sim 0.37$, as confirmed by NMR measurement. Phase separation of the PMPCS and the PS blocks was confirmed by DSC as shown in Figure 1. As previously reported, by introducing thermal hysteresis (slow cooling followed by fast heating), DSC heating thermograms clearly show two hysteresis peaks indicating two glass transition temperatures (T_g) at ~100 °C and 118 °C, corresponding to the T_g of PS and PMPCS blocks.[52] 2-D SAXS experiments were conducted on the sheared sample to confirm the phase structure. Figure 2a and b show the 2-D SAXS patterns taken with X-ray along *y* and *x* directions as defined in Scheme 1. It is evident, from Figure 2a, that, in addition to the equator diffractions, there are four strong diffractions in the quadrants. Detailed analysis shows that these four quadrant diffractions compared to the first-order

Scheme 1. Schematic Representation of the Shear Geometry of the PS-*b*-PMPCS Block Copolymers

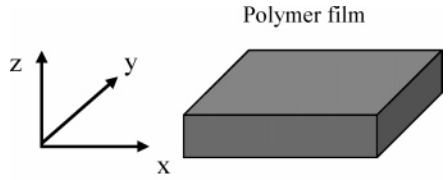

diffraction on the equator possess a slightly larger *d* spacing (24.3 and 21.3 nm, respectively), excluding the possibility of a cylindrical morphology in the BCPs. Along the equator, up to third-order diffractions can be observed. The weak quadrant diffractions, as indicated by the arrows, are attributed to the higher order of the strong quadrant diffractions. The SAXS pattern with the X-ray beam along the *x* direction is shown in Figure 2b. Interestingly, Figure 2a and b essentially possess the same feature except that higher order diffractions are absent in Figure 2b, possibly due to the relatively poor long range order along the shear (*x*) direction.

Observation of the same diffraction patterns of the sheared film along *x* and *y* directions is intriguing. It is known that, in BCP structures, mechanical shearing induces structure anisotropy in the system. In lamellar and cylinder structures, the shear direction is parallel to the lamellar layer and cylindrical axis, respectively. In the case of double gyroid and hexagonal perforated layer (HPL) structures, the shearing direction is parallel to the [111] (for $Ia\bar{3}d$ space group) and $[\bar{1}2\bar{1}0]$ (for $P6_3/mmc$ or $R\bar{3}m$ space groups) directions. Out of these four phase structures, for a single crystal-like sample, it is only in the lamellar structure that the SAXS patterns along the shearing (*x*) direction and the orthogonal (*y*) direction are identical. To obtain the in-plane symmetry of the sample, 2-D SAXS was carried out along the *z* direction and is shown in Figure 2c. A relatively weak diffraction ring can be seen with a *d* spacing of ~21 nm. From these SAXS results, we anticipate that the most possible structure is a PL phase, in which case PS and PMPCS form alternating layers and the "excessive" PS molecules punctuate the PMPCS layers. The in-plane symmetry, however, cannot be concluded. There are two possible reasons for the lack of orientation in the diffraction pattern along the *z*-direction: (1) mechanical shearing did not provide a perfect, single crystal-type structure; (2) the in-plane fluctuation is infinitely degenerated, and the diffraction pattern is intrinsically isotropic, as suggested by Laradji et al.[53]

To further confirm the PS_{171}-*b*-$PMPCS_{32}$ structure in the real space, TEM experiments were conducted on thin, ultramicrotomed films. RuO_4 was used to stain the thin BCP sections to enhance the contrast. Figure 3 shows the TEM micrographs of such films. The samples were microtomed normal to *y*, *x*, and *z* directions in Figure 3a, b, and c, respectively. It is evident from both Figure 3a and b that layer structures are formed with alternating dark (PMPCS) and light (PS) areas. It is interesting to observe that the dark areas are not continuous layers. Careful examination shows that these dark layers are formed by discrete

(52) Li, C. Y.; Tenneti, K. K.; Zhang, D.; Zhang, H.; Wan, X.; Chen, E. Q.; Zhou, Q. F.; Avila-Orta, C.; Igos, S.; Hsiao, S. *Macromolecules* **2004**, *37*, 2854−2860.

(53) Laradji, M.; Shi, A. C.; Noolandi, J.; Desai, R. C. *Macromolecules* **1997**, *30*, 3242−3255.

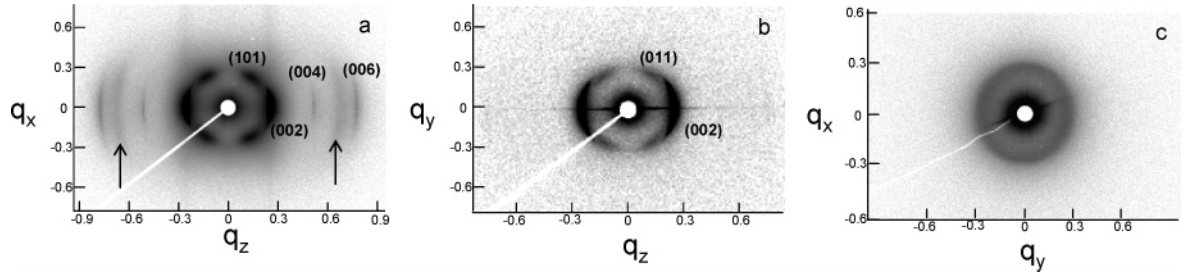

Figure 2. 2-D SAXS patterns of a PS_{171}-*b*-$PMPCS_{32}$ film with X-ray along the (a) *y*, (b) *x*, and (c) *z* direction. *X* is the shear direction as defined in Scheme 1. Arrows indicate high order diffractions of the quadrant diffractions.

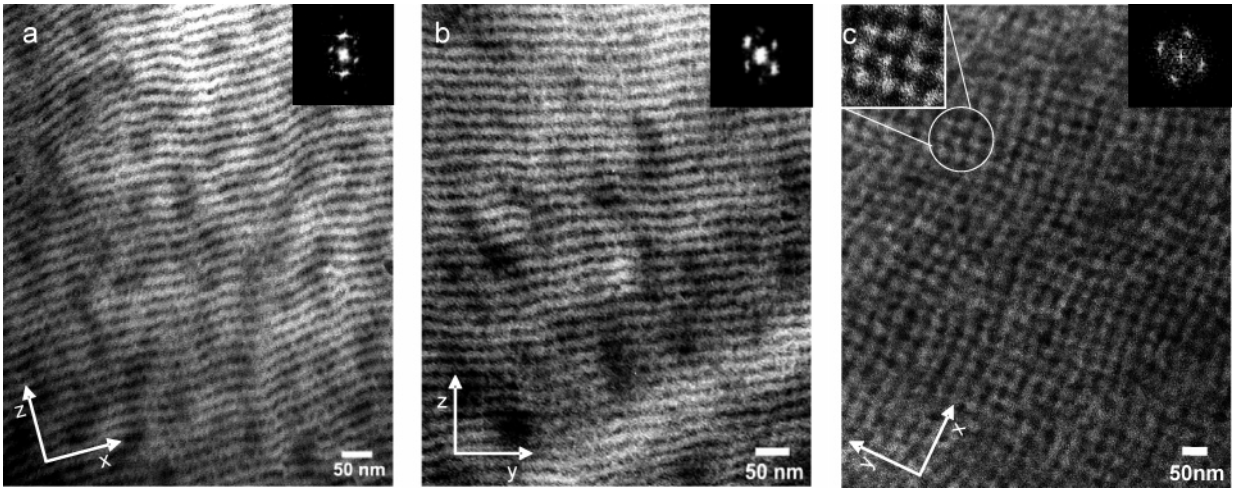

Figure 3. TEM micrographs of thin sections of PS_{171}-*b*-$PMPCS_{32}$. The sample was sectioned along the *xz* (a), *yz* (b), and *xy* (c) planes followed by RuO_4 staining for 30 min. Insets show their FFT pattern.

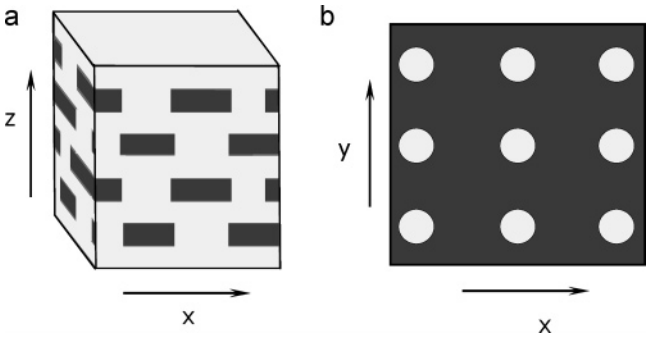

Figure 4. Schematic representation of the TPL structures viewed along the side (a) and top (b) directions.

dark spheres that are punctuated by seemingly white intersections. Similar discontinuous dark layers can be seen in both Figure 3a and b. This discontinuity of the dark layers in both *xz* and *yz* planes suggests the formation of a PL structure. Due to the large volume fraction of PS ($f^{PS} \approx 0.63$), PS punctuates the PMPCS layers and forms the perforation. TEM observation is thus consistent with the SAXS results. The in-plane symmetry of the PL phase can be unambiguously determined by viewing a thin section of the sample along the *z* direction. Since one PS−PMPCS layer is ∼21.3 nm thick, to ensure a single layer pattern, thin sections with a thickness < 15 nm were obtained and the results are shown in Figure 3c. The inset in the upper-left corner shows the enlarged image of the selected area of Figure 3c. It is evident that white PS spheres are regularly packed within the PMPCS plane, and a four-fold symmetry can be clearly seen from the micrograph. An average sphere-to-sphere distance of ∼30 nm can be estimated from the figure.

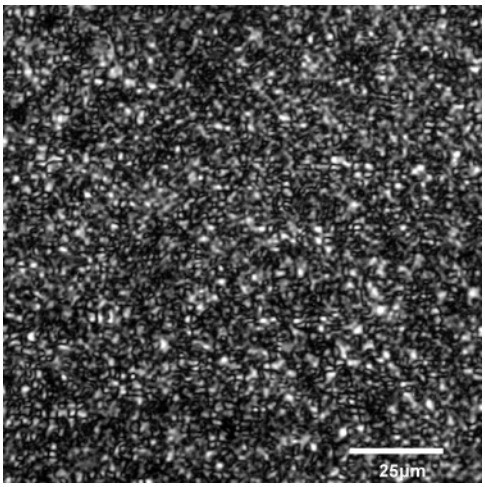

Figure 5. LC schlieren texture of PS_{171}-*b*-$PMPCS_{32}$ at 150 °C.

The upper-right corner inset shows a Fast Fourier Transform (FFT) of Figure 3c, and again, a diffraction pattern with a four-fold symmetry axis was obtained. Therefore, we can conclude that a tetragonal perforated layer (TPL) structure was formed in the PS_{171}-*b*-$PMPCS_{32}$ rod−coil BCP sample, although most of the reported PL structures in BCPs have a hexagonal symmetry (HPL).[53−58] Figure 4a shows a schematic representa-

(54) Forster, S.; Khandpur, A. K.; Zhao, J.; Bates, F. S.; Hamley, I. W.; Ryan, A. J.; Bras, W. *Macromolecules* **1994**, *27*, 6922−6935.
(55) Fredrickson, G. H. *Macromolecules* **1991**, *24*, 3456−3458.
(56) Hamley, I. W.; Bates, F. S. *J. Chem. Phys.* **1994**, *100*, 6813−6817.
(57) Qi, S. Y.; Wang, Z. G. *Macromolecules* **1997**, *30*, 4491−4497.
(58) Zhu, L.; Huang, P.; Cheng, S. Z. D.; Ge, Q.; Quirk, R. P.; Thomas, E. L.; Lotz, B.; Wittmann, J. C.; Hsiao, B. S.; Yeh, F. J.; Liu, L. Z. *Phys. Rev. Lett.* **2001**, *86*, 6030−6033.

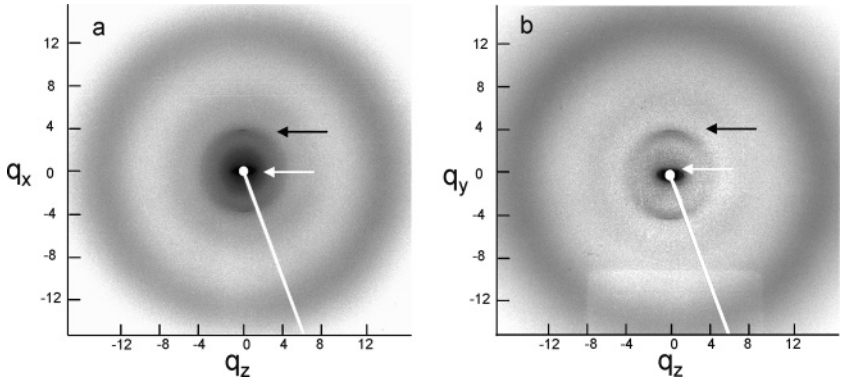

Figure 6. 2-D WAXD pattern of PS_{171}-*b*-$PMPCS_{32}$ film along (a) *y* and (b) *x* directions. Black arrows indicate the low angle diffractions along the meridian, and white arrows indicate the SAXS diffractions similar to those observed in Figure 2.

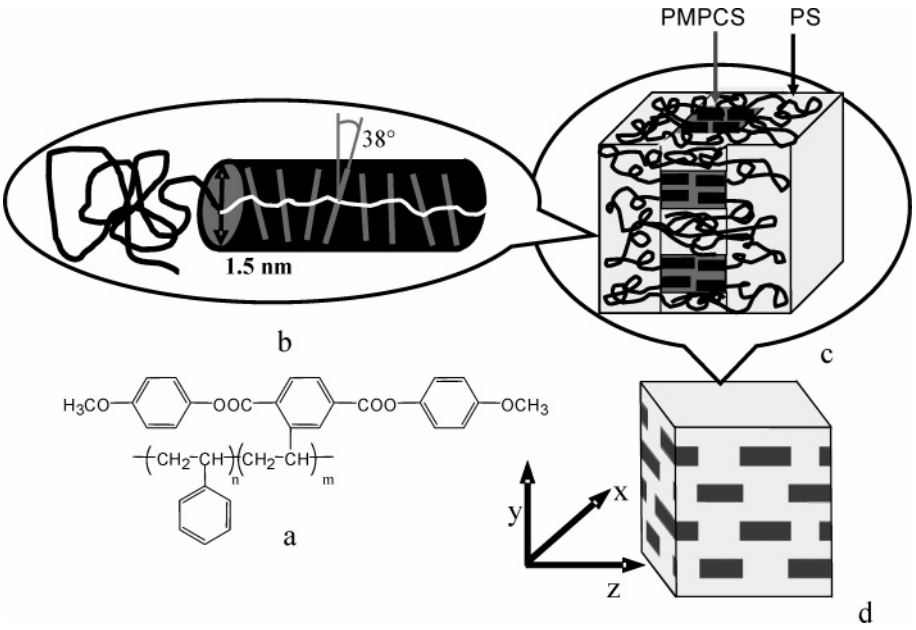

Figure 7. Schematic representations of PS-*b*-PMPCS hierarchical structure. Note the rods are parallel to the lamellar normal.

tion of the side view of the TPL structure where the dark gray color indicates the PMPCS layer and the light color indicates the PS layer. Figure 4b shows the top view of the TPL structure. Based on the TPL model, PS molecules punctuate and form isolated "islands" in the PMPCS layer, and these in-plane isolated domains obey a square lattice symmetry with $a = b =$ 29.6 nm. Therefore, the lattice of the perforation can be estimated to be $a = b = 29.6$ nm and $c = 42.7$ nm. The equator diffractions in Figure 2a can therefore be indexed as (002), (004), and (006) while the quadrant diffractions can be indexed as (101)/(011) as shown in the figure. In our previous report, we studied PS_{171}-*b*-$PMPCS_{34}$ ($f^{PS} \approx 0.62$) which possesses a lamellar structure.[52] It suggests that $f^{PS} \approx 0.63$ is on the phase boundary between lamellar and PL structures for the PS-*b*-PMPCS having 171 PS repeating units.[59] It should also be noted that HPL is known as a metastable phase which can be induced by shear. In the present study, the TPL phase might also be a metastable phase, although annealing for 3 days (at 145 °C) after shearing did not result in any change in the phase morphology.

It is intriguing to observe a tetragonal symmetry of layer perforations. To our knowledge, this is the first observation of the TPL structure in BCPs. On the other hand, theoretical work by Qi and Wang suggested that the in-plane structure of the PL phase is not necessarily hexagonal.[57] In particular, two different PL structures, one based on a hexagonal close packed (hcp) lattice and one based on a body centered cubic (bcc) lattice (ABAB..... stacking), were proposed. In the bcc based PL structures, square in-plane packing was proposed and the authors further pointed out that rectangular arrangement might also occur.[57] Our results are consistent with this prediction, and the TPL phase can be considered as a bcc PL phase "distorted" along the *c* axis. Furthermore, the TPL structure has been observed in a series of small molecular LC rod−coil/coil−rod−coil systems. It has been reported that, in a coil−rod−coil molecule of 4,4′-bis[4-methyloxypoly(propyleneoxy)propyloxy-4′-biphenyloxymethyl]biphenyl with a poly(propylene oxide) coil,[60] body-centered tetragonal liquid crystalline and crystalline phases were observed. In a similar rod−coil system, tetragonally

(59) In fact, ultramicrotomed thin sections of PS_{171}-*b*-$PMPCS_{34}$ along the lamellar normal showed a "wavy" lamellar pattern, although SAXS suggests a simple lamellar structure. This further supports that PS_{171}-*b*-$PMPCS_{34}$ is on the boundary between lamellar and PL phases. See Supporting Information for details.

(60) Lee, M.; Cho, B. K.; Jang, Y. G.; Zin, W. C. *J. Am. Chem. Soc.* **2000**, *122*, 7449−7455.

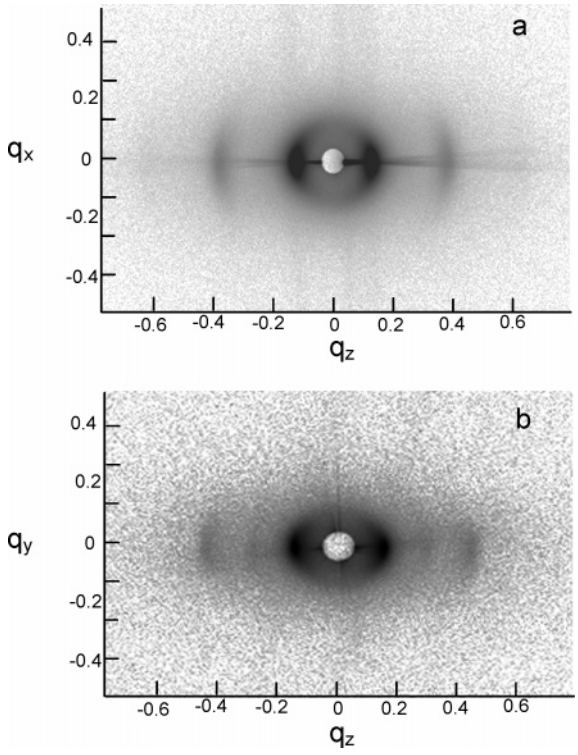

Figure 8. 2-D SAXS patterns of a PS_{272}-*b*-$PMPCS_{93}$ film with X-ray along the (a) *y* and (b) *x* directions.

perforated rod layers stacking in ABAB... order was also observed.[61] It was shown that rod−coil molecules organized into a supramolecular structure having an aromatic core with a puck-like cylindrical shape. This, in turn, leads to the formation of the oblate aggregates, which is believed to be responsible for the formation of a body-centered TPL structure, and an *I4*/*mmm* space group has been assigned to this TPL LC phase.[60,61] In the present case, observation of the TPL structure suggests that the rods that are formed by the extended macromolecules might not possess a perfect cylindrical shape, leading to symmetry breaking from hexagonal to tetragonal perforation. Although the lack of higher order diffractions prevents us from assigning a definite space group to the observed TPL structure, the four-fold tetragonal symmetry is clear, as evidenced by the TEM and SAXS experiments.

Hierarchical Structure of the LC Block Copolymers. Our previous work on low M_w symmetric samples shows that PMPCS forms a Φ_N phase and it is the macromolecular rods, instead of mesogen groups, that possess the orientational order.[52] LC phase formation in this series of asymmetric block copolymers was confirmed by PLM experiments. The Schlieren texture was observed in PS_{171}-*b*-$PMPCS_{32}$ at 150 °C and is shown in Figure 5. The block copolymer was hot pressed at 200 °C and slightly sheared to increase the monodomain size. The shear direction is parallel to one of the polarizers, and the schlieren texture is stable up to 240 °C. To investigate the orientation of the macromolecular rods within the PL structure, WAXD was conducted on the sheared film. Figure 6 shows the 2-D WAXD pattern of the PS_{171}-*b*-$PMPCS_{32}$ film along the *y* and *x* directions. Low angle diffraction arcs can be clearly seen on the meridian (dark arrows). According to our previous report, the low angle diffraction is the signature of the PMPCS rods and it represents the diameter of the macromolecular rod.[52] The diffractions correspond to a *d* spacing of ∼1.5 nm, which is consistent with the previous report. Both WAXD patterns show clearly that these low angle diffractions are located on the meridian, leading to the conclusion that the rods are parallel to the lamellar normal (for detailed analysis of the relationship between the LC rods and the WAXD pattern, see ref 52). Along the equator, we can clearly see the amorphous halo in the wide angle region, similar to our previous report. More interestingly, in the regions that are close to the beam stop, sharp diffraction arcs can be observed (white arrows) on the equator. These correspond to the SAXS diffraction arcs shown in Figure 2. Therefore, a hierarchical structure from molecular scale packing to the BCP ordering can be resolved in a single 2-D diffraction pattern. Figure 7 shows the schematic representation of the hierarchical structure of the TPL structure of PS_{171}-*b*-$PMPCS_{32}$: strong interaction between PMPCS mesogens and the backbone leads to a near extended conformation of the PMPCS, which form the rods. This rod−coil system self-assembles into the TPL structure where PS punctuates the PMPCS layers. The PMPCS rods are parallel to the layer normal of the BCP structures.

Molecular Weight Dependence of the PL Structures and the "Degree of Perforation". In the rod−coil system, M_w of the combining segments also has a substantial influence on the final phase structure. In our present study, the M_w effect on the BCPs was investigated by using PS_{272}-*b*-$PMPCS_{93}$, which possesses a symmetric volume fraction ($f^{PMPCS} \approx 0.52$) of PS with an overall molecular weight of ∼65 860 g/mol. The polymer was sheared/annealed using the same methods used for PS_{171}-*b*-$PMPCS_{32}$. Figure 8 shows the 2-D SAXS pattern along the *y* and *x* directions. The SAXS diffraction pattern suggests a lamellar structure formation in the sample. No quadrant diffractions were observed. The lamellar *d* spacing was ∼46.5 nm, which, due to the high M_w of PS_{272}-*b*-$PMPCS_{93}$, is much larger compared to that of a PS_{171}-*b*-$PMPCS_{32}$ sample (21.3 nm).

Although SAXS suggests a lamellar structure in PS_{272}-*b*-$PMPCS_{93}$, TEM experiments of ultramicrotomed sections indicate otherwise, as shown in Figure 9. Thin films sectioned normal to the *y*, *x*, and *z* directions are shown in Figure 9a, b, and c, respectively. In both Figure 9a and b, perforation of the PMPCS layer (dark region) by PS (light region) is evident. Both images are similar, and it is also of interest that, compared to Figure 2a and b, the perforation of the PS domains in the PMPCS layers is much less frequent; PMPCS forms long strips, instead of spheres, as shown in Figure 9. This possibly accounts for the "lamellae-type" diffraction pattern observed in the SAXS experiment (Figure 8) and will be further discussed in the following section. Figure 9c shows the in-plane morphology of the PMPCS layers. It is evident that PS (white) has perforated into the PMPCS layers and the in-plane packing of the PS domains is relatively random.

Observation of the limited amount of perforations in Figure 9 suggests that the structure of PS_{272}-*b*-$PMPCS_{93}$ is possibly on the phase boundary between lamellar and PL phases. To fine-tune f^{PMPCS} to confirm the PL structure formation, PS homopolymer was blended with PS_{272}-*b*-$PMPCS_{93}$. Monodispersed PS with $M_n = 5000$ g/mol was dissolved in chloroform

(61) Ryu, J. H.; Oh, N. K.; Zin, W. C.; Lee, M. *J. Am. Chem. Soc.* **2004**, *126*, 3551−3558.

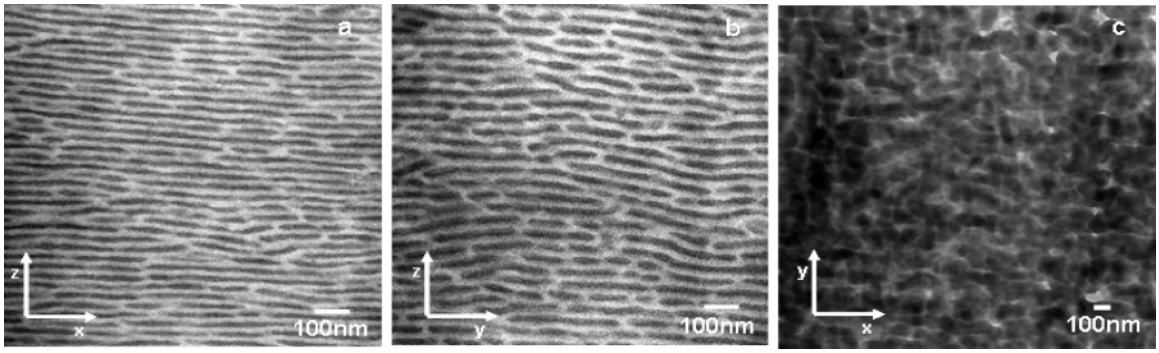

Figure 9. TEM micrographs of a thin section of PS_{272}-*b*-$PMPCS_{93}$. The sample was sectioned along the *xz* (a), *yz* (b), and *xy* (c) plane, respectively.

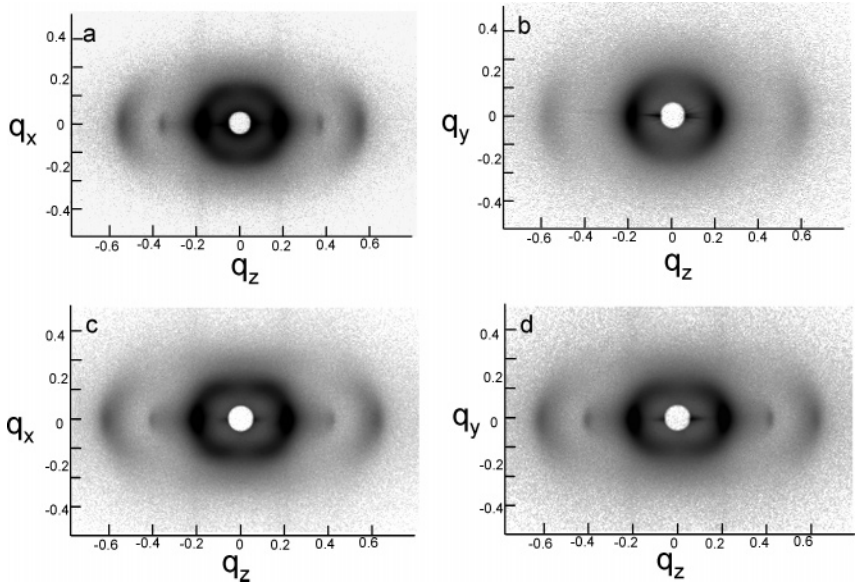

Figure 10. 2-D SAXS patterns of a PS_{272}-*b*-$PMPCS_{93}$′ film with X-ray along (a) the *y* and (b) the *x* directions and PS_{272}-*b*-$PMPCS_{93}$″ film with X-ray along (c) the *y* and (d) the *x* directions.

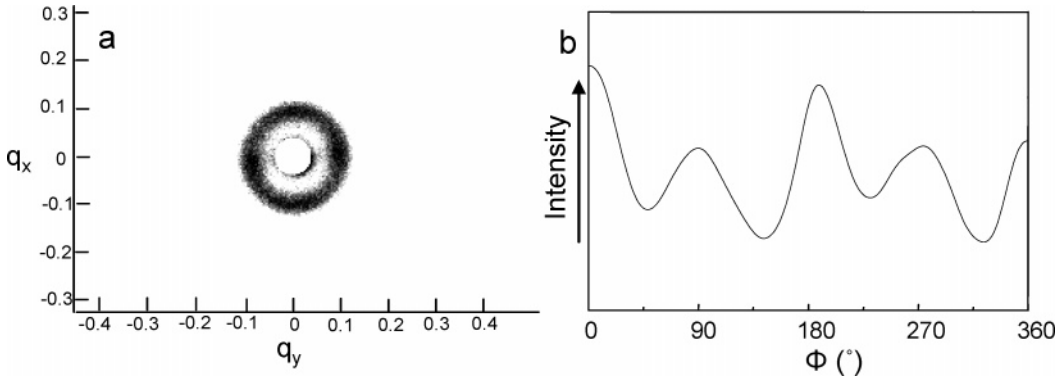

Figure 11. (a) 2-D SAXS patterns of a PS_{272}-*b*-$PMPCS_{93}$″ film with X-ray along the *z* direction. (b) The azimuthal scan of (a).

with PS_{272}-*b*-$PMPCS_{93}$ and co-solution cast to obtain polymer blend films. Low M_w PS is anticipated to mix in the PS domains and alternate the BCP morphology. Two blend samples were prepared with $f^{PMPCS} \approx 0.5$ and 0.48 and were named as PS_{272}-*b*-$PMPCS_{93}$′ and PS_{272}-*b*-$PMPCS_{93}$″, respectively. Figure 10 shows the 2-D SAXS patterns of the sheared PS_{272}-*b*-$PMPCS_{93}$′ and PS_{272}-*b*-$PMPCS_{93}$″ films along the *y* and *x* directions. Interestingly, with the addition of PS homopolymer, the *d* spacing of the first-order diffraction along the equator slightly decreased (from 46.5 to 45.2 nm to 44.4 nm). It is also evident that with decreasing f^{PMPCS} (or, increasing the f^{PS}, from PS_{272}-*b*-$PMPCS_{93}$ to PS_{272}-*b*-$PMPCS_{93}$′), the quadrant diffractions, which are the signature of the PL structure, became evident (Figure 10a). Figure 10b shows the *x* zone diffraction of PS_{272}-*b*-$PMPCS_{93}$′, whose quadrant diffractions are not as evident as that in the *y* zone pattern. However, both *x* and *y* zone diffractions from sample PS_{272}-*b*-$PMPCS_{93}$″ show strong, identical quadrant diffraction, indicating that uniform perforation occurred in the higher f^{PS} sample PS_{272}-*b*-$PMPCS_{93}$″. A 2-D SAXS experiment along the *z* direction of PS_{272}-*b*-$PMPCS_{93}$″ was also carried out, and the result is shown in Figure 11. Compared to the isotropic *z* direction SAXS pattern observed

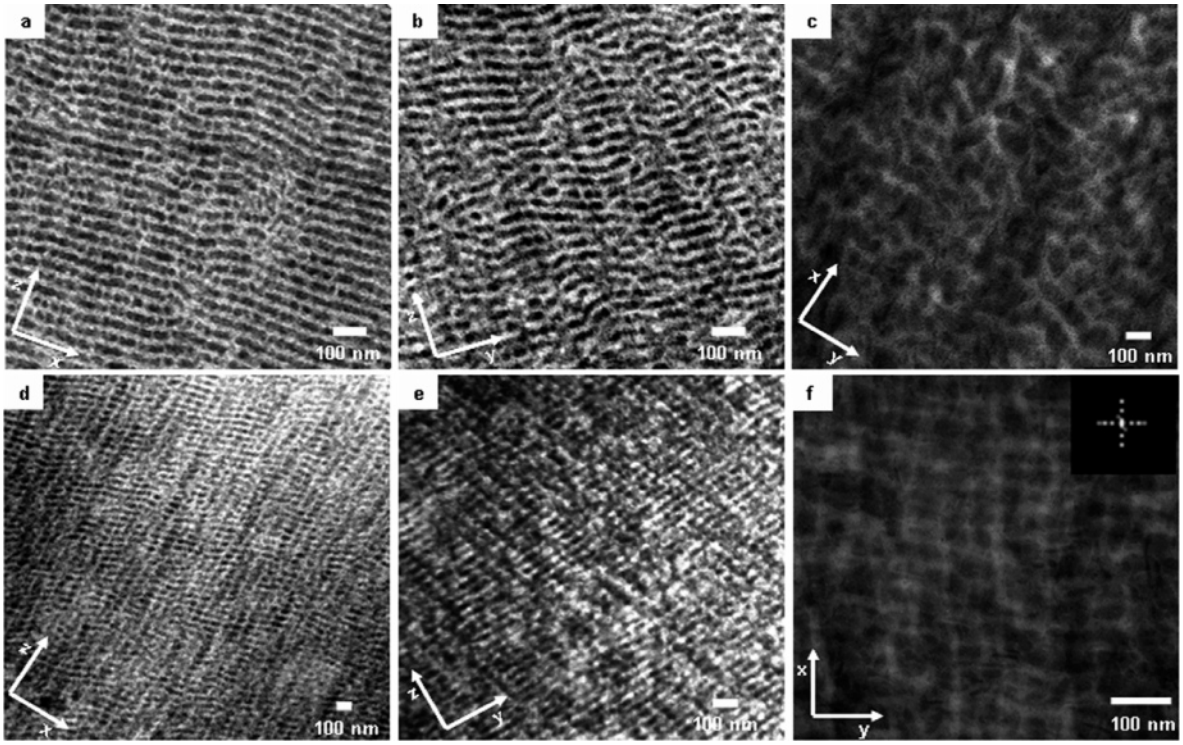

Figure 12. TEM micrographs of a thin section of PS_{272}-*b*-$PMPCS_{93}'$ (a, b, and c) and PS_{272}-*b*-$PMPCS_{93}''$ (d, e, and f). The sample was sectioned along the *xz* plane (a and d), *yz* plane (b and e), and *xy* plane (c and f).

in the low M_w PS_{171}-*b*-$PMPCS_{32}$, Figure 11a clearly shows four diffraction arcs and the azimuthal integration in Figure 11b shows that these four diffraction arcs are approximately 90° apart, indicating a four-fold symmetry. The *d* spacing of the diffraction was calculated to be ~62.3 nm. The better orientation obtained in the high M_w PS-*b*-PMPCS is possibly due to the more anisotropic fluctuation in the high M_w samples. The crystal unit cell for PS_{272}-*b*-$PMPCS_{93}''$ was calculated, and the lattice parameters are $a = b = 62.8$ nm and $c = 88.8$ nm with a tetragonal symmetry, which is consistent with our previous results in PS_{171}-*b*-$PMPCS_{32}$. Interestingly, compared to PS_{171}-*b*-$PMPCS_{32}$ (100) instead of (110) diffraction was observed, possibly due to the poor interlayer packing in the blend sample. Therefore, all the PL structures observed in the low M_w asymmetric and high M_w symmetric PS-*b*-PMPCS system obey tetragonal, instead of hexagonal, symmetry although the lattice parameters are different due to the difference in M_w. It should be noted that the lack of (200) in the *xz* plane diffraction is due to the poor long-range in-plane order of the perforated layer.

TEM experiments were carried out to view the real space features of these unique structures. Figure 12 shows the TEM micrographs of ultramicrotomed and stained sections of PS_{272}-*b*-$PMPCS_{93}'$ and PS_{272}-*b*-$PMPCS_{93}''$. The microtoming direction is perpendicular to *y* (a, d), *x* (b, e), and *z* (c, f) directions, respectively. Compared to Figure 9, morphology of these thin sections clearly changed with the addition of a small amount of PS homopolymer: long, narrow, dark strips in Figure 9a and b became relatively uniform dark spheres as shown in Figure 12a, b, d, e and the perforation in the latter is much "denser". If we define the "degree of perforation" as how frequently PS punctuates the PMPCS layers, it is evident that it continuously increases with decreasing f^{PMPCS} from 0.52 to 0.48. This also accounts for the earlier observation that the *d* spacing of the lamellar layers decreased with blending PS homopolymer. Figure 12c and f show the in-plane morphology of PMPCS layers. PS (white) perforations are again clearly seen, and more interestingly, compared to Figure 9c, the in-plane view in Figure 12c and f also shows that the perforations are denser and more regular. In Figure 12f, a square lattice can be clearly seen, which is also evidenced by the FFT of the image (inset of Figure 12f). The TPL structure can thus be further confirmed. Figure 13 shows the schematic representation of the morphological changes from lamellar to PL structure as a function of f^{PS}, viewed along *y* and *z* directions (patterns along *x* and *y* directions should be identical). Figure 13a and d represent the lamellar phase while Figure 13b, c, e, f are the PL structures. Starting from the lamellar structure, as f^{PS} increases, PS first stretches along the interface normal to accommodate the increasing f^{PS}.

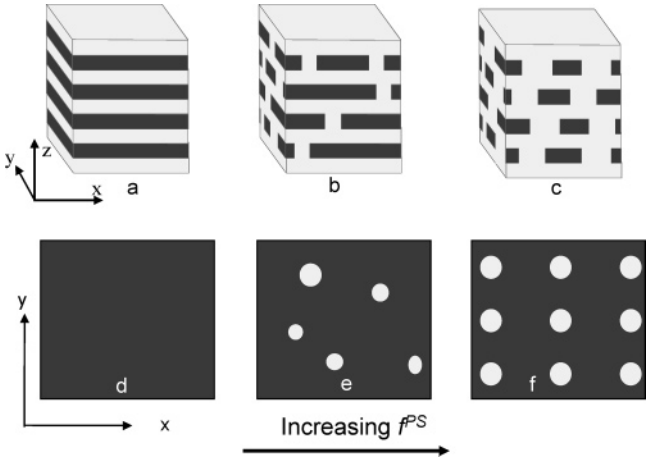

Figure 13. Schematic representation of the lamellar and TPL structures along the *y* direction (a, b, c) and *z* direction (d, e, f). Only PMPCS layers are shown in (d, e, f). The "degree of perforation" increases with f^{PS}.

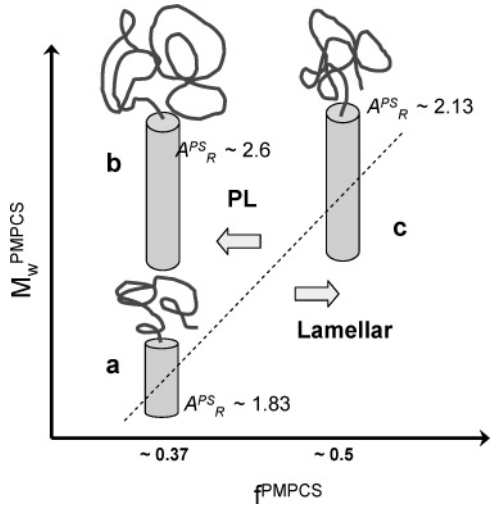

Figure 14. Schematic representation of lamellar and PL phase boundary shift with respect to M_w of the rods. (a) PS_{171}-*b*-$PMPCS_{32}$ with $A_R^{PS} \approx 1.83$, (b) PS_{497}-*b*-$PMPCS_{93}$ with $A_R^{PS} \approx 2.6$, (c) PS_{272}-*b*-$PMPCS_{93}$ with $A_R^{PS} \approx 2.13$.

This conformation change can only be tolerated to a certain degree of f^{PS}, and at this critical volume fraction of PS (f_c^{PS}), PS starts to perforate the PMPCS. At the onset of perforation, only a few PS molecules were able to punctuate through the PMPCS layer and the "degree of perforation" is low. The position of the punctuations is also random (Figures 9 and 13e). At this stage, due to the low volume fraction of PS in the PMPCS layer, regular packing of the PS "domains" was not achieved, and thus the SAXS pattern is similar to that of a normal lamellar phase. When f^{PS} increases to the perforated layer region, massive perforation occurs and PMPCS layers are broken into PS and PMPCS domains as shown in Figure 13c and f. A PL structure is therefore obtained. Note that, in Figure 13c and f, packing of the PS domains possesses a tetragonal symmetry.

It should be noted that the formation of a PL structure is consistent with the reported work on rod−coil phase structures. In rod−coil BCPs, in addition to N and χ, A^{rod} and A^{coil} play a critical role in the formation of a final structure. The rigid nature of the rod block prefers a flat IMDS rather than the highly curved ones (such as that in a double gyroid phase). In the present case, PMPCS rods are perpendicular to the IMDS of rod−coil BCPs. As long as $A^{PMPCS} \approx A^{PS}$, the lamellar structure (Sm_A or Sm_C) is stable. However, as A^{PS} becomes much larger than A^{PMPCS} (as a result of an increase in M_w), stretching of the coil polymer chain along the IMDS normal occurs and this stretching cannot accommodate the differences between A^{PMPCS} and A^{PS}. As a result, the excessive PS molecules start to punctuate the PMPCS layer, and the lamellar symmetry is broken. This PL rod−coil structure can also be viewed as the packing of a "hockey puck" structure which was predicted from theoretical calculation.[16]

Also of interest is that, in low M_w PS_{171}-*b*-$PMPCS_{32}$, the TPL structure can be observed at low f^{PMPCS} (~0.37), while, in high M_w PS_{272}-*b*-$PMPCS_{93}$, the TPL phase was observed in relatively symmetric samples ($f^{PMPCS} \approx 48\%$). This dramatic shift of phase boundary between lamellar and PL phase with M_w can be explained based on the unique packing mechanism in rod−coil BCPs as shown in Figure 14. As previously discussed, A^{rod} and A^{coil} play a critical role in the phase formation of rod−coil BCPs. The mismatch between A^{PS} and A^{PMPCS} leads to the instability of lamellar phase. We can define the "*reduced area per junction*" of the PS coil as $A_R^{PS} = A^{PS}/A^{PMPCS}$. Note that a higher A_R corresponds to a larger area per junction mismatch between coil and rod, which results in instability of the lamellar phase. We can further define the "*critical reduced area per junction*" as A_c^R which represents the area per junction ratio between the coil and the rod blocks at the phase boundary between lamellar and PL phases. The corresponding critical volume fraction is defined as f_c. In a given f^{PMPCS}, since A^{PS} increases with M_w while A^{PMPCS} does not, A_R therefore increases with M_w. In the present case, assuming strongly segregated lamellar diblocks, the area per junction of PS (A^{PS}) varies as $0.14\ M^{1/3}$ nm^2, (M: molecular weight, g/mol).[11] For PS with an M_w of 17 800 g/mol (the case of PS_{171}-*b*-$PMPCS_{32}$), A^{PS} is ~3.66 nm^2. A^{PMPCS} (which can be estimated to be ~2 nm^2) does not change with M_w. A_R^{PS} is thus approximately 1.83 (Figure 14a). Assuming a PS-*b*-PMPCS with ~93 repeating units of PMPCS (same as the sample PS_{272}-*b*-$PMPCS_{93}$), keeping $f^{PMPCS} \approx 0.37$ (as that in PS_{171}-*b*-$PMPCS_{32}$) leads to PS_{497}-*b*-$PMPCS_{93}$ (Figure 14b). A^{PS} for this sample is ~5.21 nm^2, and A_R^{PS} is ~2.6, which is much larger than 1.83, indicating a substantial area per junction mismatch between PS and PMPCS molecules. It is thus envisaged that lamellar phase is not stable at $A_R^{PS} \approx 2.6$ and the phase boundary should shift to a lower A_R^{PS}, which corresponds to a higher f_c^{PMPCS}. Our experimental observation shows that, for BCP with $PMPCS_{93}$ block, f_c^{PMPCS} shifts dramatically from 0.37 to 0.50, leading to PS_{272}-*b*-$PMPCS_{93}$ (Figure 14c) with an $A^{PS} \approx 4.27$ nm^2 and $A_R^{PS} \approx 2.13$. The dotted line in Figure 14 is a schematic representation of the phase boundary between the lamellar and PL phases. Detailed investigation is ongoing to achieve a more precise phase diagram near the lamellar and PL phase boundary.

Summary

Hierarchical self-assembly of a series of rod−coil block copolymers PS-*b*-PMPCS have been investigated. PMPCS rigid rods are formed due to the strong interaction between the side chain mesogens and the polymer backbones. The macromolecular rods possess orientational order. PL structure was observed, and the rigid rods are parallel to the lamellar normal. The packing of the PS domains in the PMPCS layer obeys a tetragonal instead of hexagonal symmetry, and TPL structure is therefore observed, possibly due to the rigid nature of the rod segments. The "onset" of perforation was observed in sample PS_{272}-*b*-$PMPCS_{93}$ whose SAXS pattern shows a "normal" lamellar diffraction while TEM images show random, low degree perforation. A slight increase in f^{PS} by blending low M_w PS homopolymers led to a dramatic change of the phase morphology, and uniform perforations were observed. The phase boundary between lamellar and PL phases was also found to be M_w dependent with $f^{PMPCS} \approx 0.37$ in relatively low M_w samples, shifting to a higher f^{PMPCS} (~0.5) as M_w increases, which is attributed to the rod−coil nature of the BCP.

Acknowledgment. This work was supported by the National Science Foundation (NSF CAREER award, DMR-0239415),

ACS-PRF, 3M, and DuPont. C.Y.L. thanks the Mettler-Toledo Co. for the Turi award supporting the thermal analysis equipment purchase. We also thank Prof. Karen Winey for the use of the ultramicrotomy equipment. X.H.W. and Q.F.Z. thank the National Natural Science Foundation of China (Nos. 20274001 and 20134010) for financial support. Synchrotron experiments were conducted at beamline X27C, NSLS in Brookhaven National Laboratory supported by DOE.

Supporting Information Available: Experimental, TEM and SAXS of PS_{171}-*b*-$PMPCS_{34}$. This material is available free of charge via the Internet at http://pubs.acs.org.

JA053548K